Title

64Cu-MM-302 Positron Emission Tomography Quantifies Variability of Enhanced Permeability and Retention of Nanoparticles in Relation to Treatment Response in Patients with Metastatic Breast Cancer

Journal

Clinical Cancer Research, 23(15)

ISSN

1078-0432

Authors

Lee, Helen
Shields, Anthony F
Siegel, Barry A
et al.

Publication Date

2017-08-01

DOI

10.1158/1078-0432.ccr-16-3193

Peer reviewed

HHS Public Access

Author manuscript

Clin Cancer Res. Author manuscript; available in PMC 2019 October 12.

Published in final edited form as:

Clin Cancer Res. 2017 August 01; 23(15): 4190–4202. doi:10.1158/1078-0432.CCR-16-3193.

^{64}Cu-MM-302 Positron Emission Tomography Quantifies Variability of Enhanced Permeability and Retention of Nanoparticles in Relation to Treatment Response in Patients with Metastatic Breast Cancer

Helen Lee[1,*], **Anthony F. Shields**[2], **Barry A. Siegel**[3], **Kathy Miller**[4], **Ian Krop**[5], **Cynthia Ma**[3], **Patricia M. LoRusso**[6], **Pamela Munster**[7], **Karen Campbell**[1], **Daniel F. Gaddy**[1], **Shannon C. Leonard**[1], **Elena Geretti**[1,†], **Stephanie Blocker**[2], **Dmitri Kirpotin**[1], **Victor Moyo**[1,†], **Thomas Wickham**[1,†], **Bart S. Hendriks**[1]

[1]Merrimack Pharmaceuticals, Inc.

[2]Karmanos Cancer Institute, Detroit, MI.

[3]Siteman Cancer Center, Washington University, St. Louis, MO.

[4]Indiana University Melvin and Bren Simon Cancer Center, Indianapolis, IN.

[5]Dana-Farber Cancer Institute, Boston, MA.

[6]Yale Cancer Center, New Haven, CT.

[7]Helen Diller Family Comprehensive Cancer Center, San Francisco, CA.

Abstract

Purpose: Therapeutic nanoparticles are designed to deliver their drug payloads through enhanced permeability and retention (EPR) in solid tumors. The extent of EPR and its variability in human tumors is highly debated and has been proposed as an explanation for variable responses to therapeutic nanoparticles in clinical studies.

Experimental Design: We assessed the EPR effect in patients using a ^{64}Cu-labeled nanoparticle, ^{64}Cu-MM-302 (^{64}Cu-labeled HER2-targeted PEGylated liposomal doxorubicin), and imaging by Positron Emission Tomography/Computed Tomography (PET/CT). Nineteen patients with HER2-positive metastatic breast cancer underwent 2–3 PET/CT scans post-administration of ^{64}Cu-MM-302 as part of a clinical trial of MM-302 plus trastuzumab with and without cyclophosphamide ().

Results: Significant background uptake of ^{64}Cu-MM-302 was observed in liver and spleen. Tumor accumulation of ^{64}Cu-MM-302 at 24–48 h varied 35-fold (0.52 to 18.5 %ID/kg) including deposition in bone and brain lesions, and was independent of systemic plasma exposure. Computational analysis quantified rates of deposition and washout, indicating peak liposome deposition at 24–48 h. Patients were classified based on ^{64}Cu-MM-302 lesion deposition using a

[*]**Corresponding Author:** Helen Lee, Merrimack Pharmaceuticals, Inc.., One Kendall Square, B7201, Cambridge, MA. 02139, (P): 617-441-7410 (F): 617-812-8122 (E): hlee@merrimack.com.

[†]Affiliation at the time of study.

cut-point that is comparable to a response threshold in preclinical studies. In a retrospective exploratory analysis of patient outcomes relating to drug levels in tumor lesions, high ^{64}Cu-MM-302 deposition was associated with more favorable treatment outcomes (hazard ratio = 0.42).

Conclusions: These findings provide important evidence and quantification of the EPR effect in human metastatic tumors, and support imaging nanoparticle deposition in tumors as a potential means to identify patients well-suited for treatment with therapeutic nanoparticles.

Keywords

^{64}Cu-liposome; PET; EPR effect; nanomedicine; tumor deposition

Introduction

Nanoparticle drug delivery systems provide a means to alter the biodistribution and pharmacokinetics of small molecule drugs. Such systems are of particular importance in oncology, where there is a need to improve the toxicity profiles and therapeutic windows for small molecule chemotherapies. Therapeutic nanoparticles can enable long-circulating pharmacokinetics and tunable sustained release and improved deposition in solid tumors through leaky vasculature. This phenomenon is referred to as the enhanced permeability and retention (EPR) effect, and is well characterized in animal models (1–3). The extent to which the EPR effect is present in human tumor lesions remains controversial but has been proposed as an explanation for variable responses to nanotherapeutics, and has important implications for the development and design of future nanomedicines (3,4).

Liposomes are a class of nanomedicines that have been proven to be clinically useful drug delivery vehicles, with several approved agents for cancer treatment (Doxil®/Caelyx®, Myocet®, DaunoXome®, Marqibo®, ONIVYDE®). The large size of liposomes, typically about 100 nm in diameter, prevents extravasation from normal vasculature and results in deposition and retention in areas of functionally porous vasculature, such as the liver and spleen, or leaky vasculature in some tumor lesions and areas of inflammation (5–7). Deposition of liposomes via the EPR effect is a non-specific phenomenon governed primarily by their size and surface characteristics (8,9).

MM-302 (HER2-targeted PEGylated liposomal doxorubicin) is a nanoparticle in clinical development for patients with HER2-positive metastatic breast cancer (,). Targeting of liposomes to tumor antigens, such as HER2, serves as means to alter the microdistribution of liposomes within tumor lesions and to direct deposited liposomes into tumors cells rather than macrophages (10). MM-302 was specifically designed to maximize doxorubicin uptake into tumor cells while minimizing uptake into non-target cells and tissues (11) and to enable combination with trastuzumab (12). While many have reported that antigen-targeted nanoparticles can lead to increased tumor uptake, the extent to which targeted nanoparticles can enhance tumor uptake is determined by many factors such as choice of targeting ligand and particle size (13–15). For some nanoparticles, tumor accumulation is independent of targeting ligand and, therefore, may be dictated primarily by the EPR effect. Previous work in preclinical models has demonstrated that the HER2-targeting did not alter overall

deposition of MM-302 into tumors (Supplementary Fig. S1), but only altered the cellular fate within the tumors (10).

Effective drug delivery is a necessary step for anti-tumor activity, and poor penetration of anticancer drugs is believed to limit the effectiveness of chemotherapy in solid tumors (16–18). As molecular size of a therapeutic agent increases, effective delivery becomes increasingly important (19). In preclinical models, effective tumor deposition of nanoparticles has also been shown to be a potentially rate-limiting step for effective drug delivery to tumor cells and the resulting anti-tumor activity (20–23).

The goal of this study was to understand the biodistribution and evaluate the potential role of the EPR effect on a nanotherapeutic in patients with metastatic breast cancer in order to determine whether tumor lesion delivery could ultimately be used to predict therapeutic efficacy. We transformed a HER2-targeted liposomal doxorubicin (MM-302) into a tracer for positron emission tomography (PET) through labeling with ^{64}Cu to enable quantitative characterization of tumor delivery kinetics. ^{64}Cu is a positron-emitting radionuclide with a 12.7 h half-life, well matched to the pharmacokinetics of MM-302. We demonstrated the clinical feasibility and safety of ^{64}Cu-liposome PET in patients. ^{64}Cu retention within liposomes was shown to be stable in patients within the image acquisition time frame. Computational modeling enabled detailed elucidation of the EPR kinetics, establishing both the deposition and washout components of tumor delivery. Variability of the EPR effect was established across lesions within a patient and across patients, as well as in non-target tissues including the liver, spleen, and bone marrow. Despite heterogeneity at the individual lesion level, we described a method of patient classification based on minimum lesion deposition and demonstrated association of tumor deposition with response to treatment.

Materials and Methods

Clinical Study Overview

Patients imaged with ^{64}Cu-MM-302 PET were part of a multi-site Phase 1 MM-302 study (). A companion imaging protocol was included after the dose escalation phase in which all patients who consented underwent ^{64}Cu-MM-302 PET. The primary objectives of the ^{64}Cu-MM-302 PET study were to determine the radiation dosimetry and biodistribution of ^{64}Cu-MM-302. The study was conducted following International Conference on Harmonization guidelines in accordance with Good Clinical Practice and the ethical principles based on the Declaration of Helsinki. The study was reviewed and approved by the local Institutional Review Board at each center prior to the start of the study and each subject gave written informed consent.

Patients

Patients enrolled in this study were ≥ 18 years of age and had advanced HER2-positive (i.e., HER2 3+ by IHC, or HER2 2+ by IHC and FISH or CISH-positive disease) breast cancer, measureable disease by RECIST v1.1, an Eastern Cooperative Oncology Group performance status of 0–1, adequate bone marrow reserves (absolute neutrophil count (ANC) ≥ 1,500/μL, platelet count ≥ 100,000/μL, hemoglobin ≥ 9 g/dL), adequate hepatic function (serum total

bilirubin within normal limits, aspartate aminotransferase (AST), alanine aminotransferase (ALT) up to 2x Upper Limit of Normal (ULN)), adequate renal function (serum creatinine ≤ 1.5 x ULN), and adequate cardiac function (left ventricular ejection fraction of ≥ 50% by echocardiography or radionuclide ventriculography). The main exclusion criteria were total cumulative doxorubicin >300 mg/m^2, active infection or unexplained fever, symptomatic brain metastases, congestive heart failure, coronary artery disease, history of myocardial infarction, hypertension, angina pectoris, valvular heart disease, severe and/or uncontrolled ventricular arrhythmia, prolonged QTc interval, history of allogeneic transplant, and infection of HIV, hepatitis B or C.

MM-302, trastuzumab, and cyclophosphamide dose

Patients imaged with ^{64}Cu-MM-302 PET were in Arms 3 and 4 of the Phase 1 study () and received the following treatment: trastuzumab at 6 mg/kg (with an 8 mg/kg loading dose on cycle 1) administered as a 90-minute IV infusion, MM-302 at 30 mg/m^2 administered as a 60-minute IV infusion, as well as a tracer dose of ^{64}Cu-MM-302 as described below. The first 3 patients of Arm 3 received trastuzumab starting on cycle 2 in order to enable initial safety assessment of ^{64}Cu-MM-302. Patients in Arm 4 also received cyclophosphamide at 450 mg/m^2 5 days prior to ^{64}Cu-MM-302 based on a preclinical study showing that tumor priming with cyclophosphamide enhanced tumor delivery of MM-302 in xenografts (24). All patients received prophylactic premedication with diphenhydramine or equivalent prior to dosing of MM-302.

^{64}Cu-MM-302 dose

^{64}Cu-MM-302 was prepared by a commercial radiopharmacy using $^{64}CuCl_2$ obtained from Washington University (St. Louis, MO USA), a chelating/loading agent (Diacetyl 4,4′-bis(3-(N,N-diethylamino)propyl)thiosemicarbazone, or 4-DEAP-ATSC), and MM-302. 2.5 mL of 0.06 mg/mL 4-DEAP-ATSC was added to $^{64}CuCl_2$ and incubated for 1 min at room temperature. The chelated ^{64}Cu mixture was passed through a 0.2 μm filter into a vial containing 5 mL of 2 mg/mL MM-302. The mixture was heated to 65°C for 10 min and then cooled to room temperature. The efficiency of loading was measured by size exclusion chromatography as previously described (25).

Quality control testing for ^{64}Cu-MM-302 consisted of total activity (400 MBq ± 10%), radiochemical purity (^{64}Cu loading efficiency ≥ 85%), appearance (red opalescent solution), endotoxin (≤ 35 EU/mL), and sterility. The effect of ^{64}Cu labeling on MM-302 was found to have negligible effects on key MM-302 characteristics (HER2-binding, doxorubicin content, phospholipid concentration) and maintain an acceptable pH for administration. Preclinical characterization and stability of ^{64}Cu-MM-302 was reported elsewhere (25).

For all patient doses, radiochemical purity was observed in the range of 95–99%. Within 3 hours after administration of 30 mg/m^2 MM-302 (doxorubicin equivalent), approximately 400 MBq of ^{64}Cu-MM-302 (approx. 3–5 mg/m^2 doxorubicin) in 3–7 mL (depending on the ^{64}Cu-labeling specific activity at the time of administration) was administered as an IV infusion over 10 min using an infusion pump, followed by a saline flush.

PET image acquisition and quantification

Each patient underwent PET/CT 0–3 h after administration of ^{64}Cu-MM-302 on Day 1 and additional scan(s) on Day 2 and/or Day 3 depending on scan group assignment upon enrollment. Five of the nineteen patients consented to all three scan times. Image acquisition times on Days 1, 2 and 3 were 3–5, 7–9 and 12–15 min per bed position, respectively. Approximately 6 bed positions were obtained for each patient, spanning from mid-brain to mid-thigh axially.

Quantification of images was performed using MIM software (MIM Software Inc.; Cleveland, OH.; Version 6.2 or higher). Rather than maximum standardized uptake value (SUV_{max}), tracer concentration was reported as the percent injected dose per kg of tissue (%ID/kg) within a region of interest (ROI), derived from SUV_{median} normalized to body weight (BW). %ID/kg is related to SUV in the following manner: %ID/kg tissue = SUV/BW*100%. This measure provides a quantitative measure of drug concentration in the ROI. It is hypothesized that drug activity will be closely related to absolute drug concentration, and for this reason, SUV_{max}, which is conventionally used to correlate with tumor metabolic activity (in the context of ^{18}F-fludeoxyglucose (FDG)) is not appropriate. The median tissue uptake was determined by creating a 3D ROI in metastatic lesions and in normal tissues (heart, lung, liver, spleen, kidneys). Tumor lesion ROIs were selected by an independent radiologist board-certified in nuclear medicine. The median radioactivity for all tumor lesions and tissues were exported from the MIM software into an electronic case report form (eCRF) for further analysis. As an exploratory analysis, bone marrow uptake was quantified using an 8 mm spherical ROI in the lumbar vertebrae (average of L1-L5). Vertebrae with bone metastases or sclerotic lesions based on CT were excluded from normal bone marrow analyses.

Safety Monitoring

Safety of the underlying chemotherapy regimen is reported elsewhere (26,27). Briefly, vital signs were monitored at multiple time points, both before and after the MM-302 and ^{64}Cu-MM-302 administrations. Hematology, liver, and kidney functions were assessed throughout the study. Continual follow-up assessment for adverse events at each study visit was in place to monitor for any possible sequelae of the radiopharmaceutical imaging study. Safety of ^{64}Cu-MM-302 as a PET tracer was established through radiation dosimetry as described below.

Radiation dosimetry

Data were presented as PET image files to an independent medical physicist with expertise in radiopharmaceutical dosimetry. Counts in tissues were extracted from the images using the MIPAV software (28). Activity in each visualized organ and the total body were expressed as fractions of injected activity, normalizing the activity in the whole body at the earliest time point to be 100% of the administered activity. Resultant values of percent of injected activity per organ were fit using the SAAM II software (29). Time integrals of activity (30) were entered into the OLINDA/EXM software (31), using the adult male model. The number of disintegrations in the ‘remainder of body’ was assumed to be that in total body within the field of view minus the values in other organs of uptake.

Tracer kinetic modeling

The tracer kinetic model used follows a general form previously presented for describing liposome transport into and out of tumors (20,32). The PK of ^{64}Cu-MM-302 was represented with a single blood compartment with volume V_c and clearance characterized by elimination rate constant k_{el}. The tumor (volume = V_t, assuming tissue density ρ = 1 kg/L) was described in a semi-physiological manner with a vascular portion and tissue portion consisting of cellular and interstitial space. The fractional volume of the tumor occupied by vasculature was described by a vascular volume fraction (VVF). Blood flow rate into and out of the tumor (Q) was assumed constant at 0.0282 L/kg/min (33). Washout of particles from the tumor, either back into the blood or via lymphatic drainage, is lumped into a single process for simplicity. Deposition and washout of ^{64}Cu-MM-302 into and out of the tumor tissue space was assumed to follow first-order kinetics and were characterized by rate constants k_1 and k_{-1}, respectively.

Equations are listed below:

$$\frac{dC_b}{dt} = \frac{1}{V_c}\left(-k_{el} \cdot C_b \cdot V_c - Q \cdot V_t \cdot \rho \cdot C_b + Q \cdot V_t \cdot \rho \cdot C_{tv}\right)$$

$$\frac{dC_{tv}}{dt} = \frac{V_t \cdot \rho}{V_t \cdot VVF}\left(Q \cdot C_b - Q \cdot C_{tv} - k_1 \cdot C_{tv} + k_{-1} \cdot C_{tt}\right)$$

$$\frac{dC_{tt}}{dt} = \frac{V_t \cdot \rho}{(1 - VVF)}\left(k_1 \cdot C_{tv} - k_{-1} \cdot C_{tt}\right)$$

$$C_{t,total} = C_{tv} \cdot VVF + C_{tt} \cdot (1 - VVF)$$

where C_b, C_{tv}, C_{tt}, $C_{t,total}$ are the concentrations of ^{64}Cu-MM-302 in the blood, tumor vasculature, tumor tissue, and total tumor, respectively. The following parameters were estimated directly from the kinetic data: k_{el}, VVF, k_1, k_{-1} using median values extracted from ROI analysis from the images and associated tumor volume measurements. Additional information on the model parameters are provided in Supplementary Table S1. The model was implemented in MATLAB (The Mathworks, Natick, MA).

Statistical Analysis

Treatment outcome was not assessed on the companion imaging protocol, but was documented under the parent protocol per RECIST v1.1 criteria. Image-based ROI analysis data was captured using an eCRF developed in compliant with 21 CFR Part 11, with the exception of the bone marrow uptake data that were obtained for additional exploratory analysis. Uptake data were then exported for further computational analyses. Statistical and PK analyses were performed using MATLAB (The Mathworks, Natick MA) or GraphPad

Prism version 6.0 (GraphPad Software, San Diego, CA). Only nonparametric statistical tests were utilized, including Mann-Whitney, Kruskal-Wallis, or Spearman Correlation, wherever applicable. Data are shown as median [interquartile range] unless otherwise indicated.

Results

It is well established that there is a dose-activity relationship for liposomal anti-cancer agents in preclinical tumor models (34). We therefore sought to identify the minimum tumor delivery of MM-302 required for anti-tumor activity in preclinical models (details described in Supplementary Materials). As expected, increased tumor delivery was observed with increasing dose (Supplementary Fig. S2A; range: 1–13 μg doxorubicin per gram of tumor tissue, or μg DOX/g). The 3 mg/kg dose level, roughly corresponds to the dose level at which MM-302 can effectively inhibit tumor growth (Supplementary Fig. S2B), resulted in a minimum tumor concentration of 2.3 μg DOX/g. Based on these findings, we sought to determine the concentrations of liposomal drug achieved in tumor lesions in patients, and hypothesized that a minimum effective dose would be necessary for effective treatment with liposomal therapies such as MM-302.

PET/CT of ^{64}Cu-MM-302 in patients

Between July 2013 and July 2014, 25 patients were dosed with MM-302 as part of a Phase 1 study (); 19 of the patients underwent ^{64}Cu-MM-302 PET. Patient demographics are shown in Supplementary Table S2. All 19 patients were imaged on Day 1 between 0.2–2h (median 0.7 h) post-administration of ^{64}Cu-MM-302; 16 and 8 patients also underwent scans on Day 2 (median of 21.2 h) and Day 3 (median of 44.6 h), respectively. A total of 5 patients had 3 PET scans on Days 1, 2, and 3 post-administration. The median age of imaged patients was 54 (range: 41–71) and the median body weight was 71.7 kg (range: 50.5–97.3 kg). Patients were enrolled into two different arms where arms 3 and 4 include treatment with trastuzumab + MM-302 and cyclophosphamide + trastuzumab + MM-302, respectively.

The mean activity of ^{64}Cu-MM-302 administered was 389 MBq (range: 337–432 MBq). The administration of ^{64}Cu-MM-302 was well tolerated by all subjects. Any study drug related adverse events recorded could not be uniquely attributed to ^{64}Cu-MM-302 because ^{64}Cu-MM-302 is administered within a few hours of MM-302, and the exposures to the two molecules overlap during the period of treatment emergent adverse event reporting.

Pharmacokinetics and Biodistribution of ^{64}Cu-MM-302

Whole-body distribution of ^{64}Cu-MM-302 is shown for two patients on Days 1–3 post-administration in Fig. 1. Immediately following administration, ^{64}Cu-MM-302 is almost exclusively localized in the blood pool, as expected for a PEGylated liposome. On Days 2–3 (19–47 h), deposition of ^{64}Cu-MM-302 was seen in the liver and spleen, but there was relatively slow clearance from the blood. Images were consistent with hepatic clearance of MM-302 and no significant uptake of the tracer was seen in the kidneys or bladder of any patients.

Decay-corrected time-activity plots for ^{64}Cu-MM-302 in selected normal tissues are shown in Fig. 2 for all patients. Because of the relatively long circulation time of ^{64}Cu-MM-302,

the presence of large blood vessels in any ROI has the potential to skew the average values within an ROI. For this reason, median activity within each ROI was used to provide a more robust measure of tissue uptake. There was very little uptake in normal muscle and normal lung tissue (< 6 %ID/kg). Median normal liver uptake was approximately 6.5 [5.2–7.3] %ID/kg post-administration and increased with time to 15.7 [12.4–21.8] %ID/kg on Day 3 (decay-corrected). Uptake into normal spleen appeared to be the most variable with 10.5 [8.6–13.3] %ID/kg post-administration, with a mild increase to 17.0 [13.5–18.3] and 13.2 [7.8–19.6] %ID/kg on Days 2 and 3, respectively. ^{64}Cu-MM-302 uptake was also observed in the bone marrow, peaking between Days 2–3 at 4.2 [3.6–4.7] and 3.6 [2.0–4.0] %ID/kg, with similar uptake kinetics as normal spleen; this is consistent with the expected uptake of nanoparticles by the reticuloendothelial system (RES) (35). Although the level of uptake in bone marrow seems to be on par with that of lung tissue, the kinetics of bone marrow uptake resemble that seen in the liver/spleen instead of the constant decrease observed for muscle and lung (i.e., blood clearance).

The behavior of ^{64}Cu-MM-302 in the blood pool was assessed from PET/CT images using an ROI in the aorta and is shown in Fig. 2F and G. The clearance of ^{64}Cu-MM-302 was highly reproducible and consistent with mono-exponential clearance kinetics previously reported for MM-302 based on doxorubicin content (26,27). Mono-exponential clearance kinetics made it possible to determine estimates of the pharmacokinetic parameters from the 2–3 images obtained per patient. Estimation of pharmacokinetic parameters (compartment model) from the imaging data (mean $t_{1/2}$ = 33 h) compared well with the 39 h (95% CI = 29–53 h; n=10) half-life reported for MM-302 at the 30 mg/m^2 dose level (26). One patient had significantly faster blood clearance ($t_{1/2}$ = 9.53 h) with significant sequestration of ^{64}Cu-MM-302 at 0.5 h in the liver and spleen (Supplementary Fig. S3). This patient was in Arm 4 (with cyclophosphamide treatment) but rapid clearance does not seem to be attributed to cyclophosphamide, as the blood $t_{1/2}$ was not significantly different in Arm 3 without cyclophosphamide (median $t_{1/2}$ = 36.5 [23.6–44.3] h) compared to Arm 4 (median $t_{1/2}$ = 35.4 [25.2–40.9] h; p = 0.97). Most normal tissue uptake between the two groups were also comparable, with the exception of muscle on Day 1 (Arm 3 = 1.9[0.6–1.3] %ID/kg vs. Arm 4 = 0.6[0.3–0.8] h; p = 0.027) and bone marrow on Day 2 (Arm 3 = 4.3[4.1–5.4] %ID/kg vs. Arm 4 = 3.9[2.9–4.4] h; p = 0.042) where Arm 3 patients have higher uptake.

The stability of ^{64}Cu labeling of MM-302 was assessed in 3 patients. Free ^{64}Cu was not detectable above background any time point (Supplementary Fig. S4), indicating highly stable labeling of MM-302 with ^{64}Cu. In addition, almost all the ^{64}Cu activity remained in the serum component, with <4% ^{64}Cu detected in blood cells. These results were consistent with preclinical development of the ^{64}Cu-MM-302 labeling method (25).

Radiation Dosimetry

Internal radiation dosimetry was evaluated in a subset of patients (n=11). The target radioactivity was 400 MBq, and the median radioactivity administered to the 11 patients for radiation dosimetry analysis was 389 (range: 337–432) MBq. The mean estimated radiation absorbed dose for each organ, effective dose and total body dose are shown in Supplementary Table S3. The highest absorbed radiation dose was in the heart wall,

followed by the spleen, and liver receiving 0.25 [0.20–0.31], 0.12 [0.09–0.21], and 0.09 [0.09–0.12] mGy/MBq, respectively. The median effective dose was 0.028 mSv/MBq.

Tumor lesions uptake of ^{64}Cu-MM-302

Tumor lesions could be visualized on Days 2 and 3 of ^{64}Cu-MM-302 PET scans (Fig. 3). Similar to normal tissue uptake, there was no significant difference in lesion uptake for patients treated vs. not treated with cyclophosphamide (Arm 3 vs. 4, $p \geq 0.67$ for all 3 scans) (Fig. 4A). Based on these findings, subsequent analyses were performed by combining data from the two treatment arms. Increasing activity in tumor lesions were noted from the initial scan on Day 1 to Days 2–3 scans at varying degrees (Fig. 4B) while the activity in the blood decreased over this time frame (Fig. 2F). In the initial scan, median ^{64}Cu-MM-302 signal in lesions was 2.3 %ID/kg (range: 0.24–7.1 %ID/kg, n=68 lesions), reflecting predominantly tumor blood pool. Comparison with blood measurements yield a ratio of 0.13, which is consistent with the expected tumor vascular volume fraction determined by other methods (36–38). The median tumor-to-blood ratios were 0.080 [0.045–0.120], 0.208 [0.082–0.188], and 0.468 [0.111–0.451] on Days 1, 2, and 3, respectively. There were a few lesions that showed either no change or a decrease in signal over time, but did not decrease as rapidly as the blood pool signal, still suggesting a small degree of ^{64}Cu-MM-302 deposition. Median ^{64}Cu-MM-302 deposition on Days 2 and 3 were 3.7 [2.8–7.5] and 4.0 [2.3–10.6] %ID/kg indicating no significant differences in lesion uptake between Day 2 and Day 3.

Based on the known ^{64}Cu-to-doxorubicin ratio, it is estimated that the tumor deposition of MM-302 on Days 2–3 range from 0.22 to 11 μg DOX/g. 90% of the patient lesions had deposition that are consistent with the range of MM-302 tumor uptake in preclinical xenograft models (Supplementary Fig. S2A, range: 1–13 μg DOX/g). ^{64}Cu-MM-302 uptake was heterogeneous within each patient among multiple lesions (Fig. 4C). The extent to which ^{64}Cu-MM-302 accumulates in individual lesions is therefore unique to the lesion characteristics rather than the pharmacokinetics of ^{64}Cu-MM-302, as lesion uptake on Days 2 or 3 was not correlated with exposure ($p > 0.08$, Pearson Correlation with blood $AUC_{0\rightarrow\infty}$; Fig. 4D). There was also no significant correlation between lesion signal and lesion volume ($p > 0.27$) for Scan 2 or 3 (Fig. 4E).

Uptake was observed in lesions of various anatomical locations, including the lung, brain, lymph nodes and bone, as shown in Fig. 3 with deposition quantification presented in Fig. 4F. Hepatic lesions primarily appeared as hypo-active regions, because of the high background activity of the liver, but showed evidence of signal enhancement over time. There were also several instances where hepatic lesions had uptake similar to that of normal liver tissue, requiring reference to contrast-enhanced diagnostic CT to guide ROI selection (Supplementary Fig. S5). In all 3 scan time points, hepatic lesions were consistently higher than other anatomical locations (Fig. 4F; $p < 0.0001$ on Days 2 and 3; only anatomical locations with more than 3 data points were included in statistical analyses).

Kinetics of ^{64}Cu-MM-302 tumor deposition

In patients who consented to undergo 3 scans, a detailed kinetic analysis of ^{64}Cu-MM-302 in tumor lesions was possible. Fig. 5 shows the ^{64}Cu-MM-302 lesion deposition kinetic

profiles of a patient, who had 4 tumor lesions that were selected for analysis by the independent reviewer. Quantification of ^{64}Cu-MM-302 uptake for the individual lesions is shown in Fig. 5A. A chest wall lesion showed comparatively high uptake on Day 3 while the two hepatic lesions and one neck lesion had comparatively lower uptake. Images corresponding to comparatively high (ROI 3) versus low (ROI 4) uptake lesions are shown in Fig. 5B.

Three imaging data points and a basic set of assumptions regarding ^{64}Cu-MM-302 transport (see Materials and Methods) enabled elucidation of the full kinetics of ^{64}Cu-MM-302 deposition into and out of the tumor lesions including determination of the contribution of blood versus tissue-deposited ^{64}Cu-MM-302. A schematic of the tracer kinetic model used is shown in Fig. 5C. The model assumes first-order clearance of ^{64}Cu-MM-302 from the central blood pool and a fixed rate of convective transport (blood flow) from the central compartment into the vascular compartment of the tumor. The tumor is characterized by a vascular volume fraction and ^{64}Cu-MM-302 transport from the vascular compartment into the tissue, through a combination of convective and diffusive transport, is characterized by a first-order rate constant. Washout of ^{64}Cu-MM-302 is also assumed to follow first-order kinetics. Cellular uptake and processing of ^{64}Cu-MM-302 is also assumed to be minimal over the 3-day time scale of imaging. Shown in Fig. 5D, the kinetic model was fit to the blood and tumor data, demonstrating that this model framework was able to quantify the inter-lesion heterogeneity of uptake through variations in rates of deposition, washout, and vascular volume fraction (Supplementary Fig. S6). The model results indicate peak deposition of MM-302 in human tumors occurs on approximately Days 2–3 and supports the selected imaging times used. The fraction of tumor ^{64}Cu-MM-302 signal on Days 2–3 arising from the vascular versus deposited ^{64}Cu-MM-302 was minimal compared to the tumor tissue signal, suggesting that most ^{64}Cu tumor signal after Day 1 is attributed to deposition of ^{64}Cu-MM-302 in the tumor tissue.

Patient classification and association with treatment outcome.

Inadequate drug delivery to a single tumor lesion within a patient may be sufficient to result in progressive disease when patients are evaluated based on RECIST v1.1. For this reason, we classified patients into two groups based on their lowest uptake lesion. At approximately 2 %ID/kg, a plateau was observed based upon the distribution of lowest uptake lesion deposition of each patient (Fig. 6A). Tracer deposition of 2 %ID/kg corresponds to approximately 1.2 μg DOX/g, which is comparable to the preclinical effective threshold established previously (2.3 μg DOX/g; Supplementary Fig. S2).

Although not a formal objective of the study, a preliminary retrospective analysis was attempted to correlate ^{64}Cu-MM-302 lesion uptake and patient response to treatment. The best overall responses per RECIST v1.1 for the two groups classified based on imaging data are shown in Fig. 6B to D. 75% of subjects experienced a partial response (PR) and/or stable disease (SD) in the high deposition group, while 43% of patients experienced SD with no PR in the low deposition group. The patients in groups with the low and high ^{64}Cu-liposome deposition lesions had median progression free survival (PFS) of 1.7 and 2.0 months, respectively, with a hazard ratio of 0.42 (logrank method). ROC analysis of the minimum

lesion uptake against PFS yielded a deposition threshold of 2.4 %ID/kg, which resulted in the same patient stratification. The limited number of imaged patients on each treatment arm with analyzable RECIST data (n= 9 and 10 for Arms 3 and 4, respectively) precluded a meaningful statistical comparison.

Discussion

The extent of therapeutic nanoparticle deposition in solid tumors is a vital component of establishing local drug concentrations and the overall therapeutic window. Understanding the extent and variability of the EPR effect in patient tumors is at the core of understanding whether local drug levels are limiting in patient responses to therapeutic nanoparticles (3). While preclinical examples exist, this simple pharmacological concept has been difficult to translate into the clinical setting (39).

In this study, we utilized preclinical models to identify a minimum critical concentration threshold of MM-302 tumor delivery required to control tumor growth and translated this concept into a clinical study. We hypothesized that tumor lesion delivery of therapeutic nanoparticles such as MM-302 are highly variable, and locally achievable drug concentrations span critical thresholds that determine sensitivity versus lack of response. In order to test this hypothesis, we transformed MM-302 into a PET tracer through ^{64}Cu-labeling and incorporated imaging with ^{64}Cu-MM-302 PET/CT into a clinical trial of MM-302 plus trastuzumab with or without cyclophosphamide. Patient tumor concentrations of MM-302, as determined with ^{64}Cu-MM-302, were remarkably consistent with those determined from preclinical data, and span a range of concentrations that potentially impact therapeutic responses. Our results have important implications for clinical development of therapeutic nanoparticles.

To date, patients with cancer have been imaged in several clinical studies with ^{111}In-liposomes or ^{99m}Tc-liposomes via planar scintigraphy or single-photon emission computed tomography (SPECT) to assess tumor uptake of the liposomes (40–43). However, these clinical studies were limited to visualization or semi-quantitative analysis of liposome behavior because of the limitations of the imaging methods and/or the short half-life of the radionuclide tracer. Relative to SPECT, PET has the advantage of increased sensitivity and spatial resolution while allowing for straightforward data quantification and whole-body 3D imaging.

The kinetic nature of our studies with ^{64}Cu-MM-302, coupled with the accuracy afforded by PET/CT, clearly establish that the EPR effect is present in human metastatic tumors. The accumulation of ^{64}Cu-MM-302 in tumor lesions over time was not observed in normal tissues such as muscle, and is consistent with the EPR effect of nanoparticles as reported in the literature (44,45). The data indicate the variable nature of this process, not only in terms of deposition rates but washout rates as well. Rates of deposition and washout determined from human tumors compared well with rates estimated from mouse xenograft models (20). Further, kinetic modeling indicated that at later times the ^{64}Cu signal was predominantly the result of tissue-deposited liposomes. By contrast, early imaging times, as used in ^{99m}Tc-

liposomes studies, are largely a measurement of tumor lesion vascular volume fraction (41–43).

This study also highlights the interplay between normal liver and hepatic tumor lesions for therapeutic nanoparticles. As expected, the liver was a site of high background signal because of its role in metabolizing and clearing liposomes. By contrast, little to no signal was observed in the kidney or bladder, supporting the stability of the ^{64}Cu-MM-302 tracer, as well as the liver being the primary route of clearance. The liver is also a common site of metastatic disease in breast and other cancers. Hepatic lesions were able to be visualized in most cases as they tend to appear as hypo-active regions relative to the high normal tissue uptake background. In some cases, where hepatic lesion uptake was similar to normal liver tissue, diagnostic CT was required to help delineate the liver-lesion boundary. The spatial resolution of PET and partial volume effects make accurate quantification of these lesions difficult. This may be particularly true for lesions with an actively growing rim and/or necrotic core. Similarly, lesions with significant fibrosis or scar tissue may also be difficult to resolve from actively growing lesions by CT. For these reasons, comparison of ^{64}Cu-MM-302 PET with ^{18}F-FDG PET would be an interesting future direction for identifying metabolically active lesions to further the understanding of liposome tumor deposition.

The data presented herein provide evidence supporting a mechanism by which ^{64}Cu-MM-302 liposomes deposit and accumulate in human tumors. An interesting and serendipitous finding of this study was the accumulation of ^{64}Cu-MM-302 in brain lesions. The delivery of large molecules to brain lesions has been previously shown by imaging with liposomes (41) and ^{64}Cu-/^{89}Zr-labeled trastuzumab (46,47). Similarly, Siegal *et al.* had reported a 14-fold increase in liposomal doxorubicin delivery to brain tumor in a mouse model compared to adjacent normal brain tissue (48). This almost certainly reflects disruption of the blood-tumor-barrier in metastatic lesions, rather than large liposomes traversing the blood-brain-barrier directly. Greater disruption would be predicted to lead to increased delivery and might determine the extent of response to therapy (49,50).

Variable ^{64}Cu-MM-302 uptake occurred both across lesions within a patient and across patients. In general, in patients with multiple lesions, not all of the lesions had the same level of uptake. This suggests that patient classification based on nanoparticle delivery is potentially complex, and cannot be solely determined by systemic exposure. However, patient lesion data can be classified into two groups: (i) variable uptake including low-uptake lesions, and (ii) variable uptake with only high-uptake lesions, based on the rationale that poor delivery to a single lesion could be sufficient to presage disease progression. Classification based on imaging data selected about one-third of patients as “low uptake” and enabled a subsequent exploratory analysis of patient outcomes. Although our retrospective analysis illustrates that patient level classification based on lesion delivery is possible and was consistent with our delivery-based hypothesis, these results are limited by the small sample size of this Phase 1 study among other factors, including the inherent chemosensitivity. For instance, patient classification was performed based on the imaging data only; however, some patients received cyclophosphamide and others did not. Nonetheless, we did not find a systematic difference in lesion uptake between lesions that

were treated with cyclophosphamide versus those that were not, suggesting this was not a primary factor in dictating outcome.

The significance of this work also extends to an improved understanding of safety. EPR effect also occurs in bone marrow and explains well-known hematological toxicities of therapeutic nanoparticles such as liposomal doxorubicin. Interestingly, less variability in uptake was observed in bone marrow than in tumor lesions, in general. This implies that the primary opportunity for patient selection lies in identifying patients based on uptake in tumor lesions rather than safety.

Together, these data suggest that it may be possible to use pretreatment imaging of nanoparticle deposition in tumors as a potential means to identify patients most likely to benefit from treatment with therapeutic nanoparticles. Future directions include development of potential diagnostic imaging agents specifically designed to assess tumor delivery of therapeutic nanoparticles. These agents would enable a comprehensive understanding of the delivery of nanomedicines to tumor lesions as a function of indication and anatomical location. Identification of patient characteristics correlating with effective nanoparticle delivery has potential to greatly benefit patients and dramatically influence clinical development decisions. Prospectively defined clinical trials will be needed to formally establish the relationships between therapeutic nanoparticle tumor delivery and treatment outcome.

Supplementary Material

Refer to Web version on PubMed Central for supplementary material.

Acknowledgments:

We thank the patients and the clinical staff for their participation and support of the study. We also thank Shari Rabenstine and Paul Galette from ICON Medical Imaging for their excellent study support, image interpretation and fruitful discussions. Tom Voller from Washington University has been tremendously helpful in coordinating logistics and supply of ^{64}Cu for the clinical study. We would like to acknowledge Cardinal Health for their role in preparation and distribution of ^{64}Cu-MM-302 to clinical sites. We also appreciate Dr. Michael Stabin's participation in the radiation dosimetry analysis. Lastly, we would like to thank Jonathan Fitzgerald, Istvan Molnar, Ty McClure, and Ulrik Nielsen from Merrimack Pharmaceuticals for their helpful input.

Financial Support: Merrimack employees receive salaries and stock options from Merrimack Pharmaceuticals. This study was solely funded by Merrimack Pharmaceuticals.

Authors affiliated with Merrimack Pharmaceuticals as indicated are employees of Merrimack Pharmaceuticals (current or at the time of study). Other authors who have received research funding from Merrimack Pharmaceuticals have made disclosure in their respective electronic conflict of interest forms.

References:

1. Matsumura Y, Maeda H. A new concept for macromolecular therapeutics in cancer chemotherapy: mechanism of tumoritropic accumulation of proteins and the antitumor agent smancs. Cancer Res. 1986;46:6387–92. [PubMed: 2946403]
2. Zheng J, Jaffray D, Allen C. Quantitative CT imaging of the spatial and temporal distribution of liposomes in a rabbit tumor model. Mol Pharm. 2009;6:571–80. [PubMed: 19298061]

3. Prabhakar U, Blakey DC, Maeda H, Jain RK, Sevick-Muraca EM, Zamboni WC, et al. Challenges and key considerations of the enhanced permeability and retention effect (EPR) for nanomedicine drug delivery in oncology. Cancer Res. 2013; 73:2412–7. [PubMed: 23423979]

4. Maeda H. Toward a full understanding of the EPR effect in primary and metastatic tumors as well as issues related to its heterogeneity. Adv Drug Deliv Rev. 2015;2–5.

5. Hansen AE, Petersen AL, Henriksen JR, Boerresen B, Rasmussen P, Elema DR, et al. Positron Emission Tomography Based Elucidation of the Enhanced Permeability and Retention Effect in Dogs with Cancer Using Copper-64 Liposomes. ACS Nano. 2015;9:6985–95. [PubMed: 26022907]

6. Greish K. Enhanced permeability and retention of macromolecular drugs in solid tumors: a royal gate for targeted anticancer nanomedicines. J Drug Target. 15:457–64. [PubMed: 17671892]

7. Nehoff H, Parayath NN, Domanovitch L, Taurin S, Greish K. Nanomedicine for drug targeting: strategies beyond the enhanced permeability and retention effect. Int J Nanomedicine. 2014;9:2539–55. [PubMed: 24904213]

8. Drummond Meyer O, Hong K, Kirpotin DB, Papahadjopoulos D. Optimizing liposomes for delivery of chemotherapeutic agents to solid tumors. Pharmacol Rev. 1999;51:691–743. [PubMed: 10581328]

9. Bertrand N, Wu J, Xu X, Kamaly N, Farokhzad OC. Cancer nanotechnology: The impact of passive and active targeting in the era of modern cancer biology. Adv Drug Deliv Rev. 2013;66:2–25. [PubMed: 24270007]

10. Kirpotin DB, Drummond DC, Shao Y, Shalaby MR, Hong K, Nielsen UB, et al. Antibody targeting of long-circulating lipidic nanoparticles does not increase tumor localization but does increase internalization in animal models. Cancer Res. 2006;66:6732–40. [PubMed: 16818648]

11. Reynolds JG, Geretti E, Hendriks BS, Lee H, Leonard SC, Klinz SG, et al. HER2-targeted liposomal doxorubicin displays enhanced anti-tumorigenic effects without associated cardiotoxicity. Toxicol Appl Pharmacol. 2012;262:1–10. [PubMed: 22676972]

12. Espelin CW, Leonard SC, Geretti E, Wickham TJ, Hendriks BS. Dual HER2 Targeting with Trastuzumab and Liposomal-Encapsulated Doxorubicin (MM-302) Demonstrates Synergistic Antitumor Activity in Breast and Gastric Cancer. Cancer Res. 2016;76:1517–27. [PubMed: 26759238]

13. Pirollo KF, Chang EH. Does a targeting ligand influence nanoparticle tumor localization or uptake? Trends Biotechnol. 2008;26:552–8. [PubMed: 18722682]

14. Hong M, Zhu S, Jiang Y, Tang G, Pei Y. Efficient tumor targeting of hydroxycamptothecin loaded PEGylated niosomes modified with transferrin. J Control Release. 2009;133:96–102. [PubMed: 18840485]

15. Duskey JT, Rice KG. Nanoparticle ligand presentation for targeting solid tumors. AAPS PharmSciTech. 2014;15:1345–54. [PubMed: 24927668]

16. Tunggal JK, Cowan DS, Shaikh H, Tannock IF. Penetration of anticancer drugs through solid tissue: a factor that limits the effectiveness of chemotherapy for solid tumors. Clin Cancer Res. 1999;5:1583–6. [PubMed: 10389947]

17. Hsueh W-A, Kesner AL, Gangloff A, Pegram MD, Beryt M, Czernin J, et al. Predicting chemotherapy response to paclitaxel with 18F-Fluoropaclitaxel and PET. J Nucl Med. 2006;47:1995–9. [PubMed: 17138742]

18. Kesner AL, Hsueh W-A, Htet NL, Pio BS, Czernin J, Pegram MD, et al. Biodistribution and predictive value of 18F-fluorocyclophosphamide in mice bearing human breast cancer xenografts. J Nucl Med. 2007;48:2021–7. [PubMed: 18006620]

19. Schmidt MM, Wittrup KD. A modeling analysis of the effects of molecular size and binding affinity on tumor targeting. Mol Cancer Ther. 2009;8:2861–71. [PubMed: 19825804]

20. Hendriks BS, Reynolds JG, Klinz SG, Geretti E, Lee H, Leonard SC, et al. Multiscale kinetic modeling of liposomal Doxorubicin delivery quantifies the role of tumor and drug-specific parameters in local delivery to tumors. CPT pharmacometrics Syst Pharmacol. 2012;1:e15. [PubMed: 23835797]

21. Karathanasis E, Suryanarayanan S, Balusu SR, McNeeley K, Sechopoulos I, Karellas A, et al. Imaging nanoprobe for prediction of outcome of nanoparticle chemotherapy by using mammography. Radiology. 2009;250:398–406. [PubMed: 19188313]

22. Pérez-Medina C, Abdel-Atti D, Tang J, Zhao Y, Fayad Z a, Lewis JS, et al. Nanoreporter PET predicts the efficacy of anti-cancer nanotherapy. Nat Commun. 2016;7:11838. [PubMed: 27319780]
23. Miller MA, Gadde S, Pfirschke C, Engblom C, Sprachman MM, Kohler RH, et al. Predicting therapeutic nanomedicine efficacy using a companion magnetic resonance imaging nanoparticle. Sci Transl Med. 2015;7:1–13.
24. Geretti E, Leonard SC, Dumont N, Lee H, Zheng J, De Souza R, et al. Cyclophosphamide-Mediated Tumor Priming for Enhanced Delivery and Antitumor Activity of HER2-Targeted Liposomal Doxorubicin (MM-302). Mol Cancer Ther. 2015;14:2060–71. [PubMed: 26162690]
25. Lee H, Zheng J, Gaddy D, Orcutt KD, Leonard S, Geretti E, et al. A gradient-loadable ^{64}Cu-chelator for quantifying tumor deposition kinetics of nanoliposomal therapeutics by positron emission tomography. Nanomedicine. 2014;1–11.
26. Lorusso P, Krop IE, Miller K, Ma C, Siegel BA, Shields AF, et al. A Phase 1 study of MM-302, a HER2-targeted PEGylated liposomal doxorubicin, in patients with HER2-positive metastatic breast cancer (MBC). Am Assoc Cancer Res Annu Meet. 2015;
27. Munster P, Miller K, Krop IE, Dhindsa N, Niyikiza C, Odueyungbo A, et al. A Phase 1 Study of MM-302, a HER2-targeted Liposomal Doxorubicin, in Patients with Advanced HER2-positive (HER2+) Breast Cancer. San Antonio Breast Cancer Symp. 2012;P5–18–09.
28. McAuliffe MJ, Lalonde FM, McGarry D, Gandler W, Csaky K, Trus BL. Medical Image Processing, Analysis and Visualization in clinical research. Proc 14th IEEE Symp Comput Med Syst CBMS 2001. IEEE Comput. Soc; page 381–6.
29. Foster DM. Developing and testing integrated multicompartment models to describe a single-input multiple-output study using the SAAM II software system. Adv Exp Med Biol. 1998;445:59–78. [PubMed: 9781382]
30. Stabin MG, Siegel JA. Physical models and dose factors for use in internal dose assessment. Health Phys. 2003;85:294–310. [PubMed: 12938720]
31. Stabin MG, Sparks RB, Crowe E. OLINDA/EXM: the second-generation personal computer software for internal dose assessment in nuclear medicine. J Nucl Med. 2005;46:1023–7. [PubMed: 15937315]
32. Gaddy DF, Lee H, Zheng J, Jaffray D a, Wickham TJ, Hendriks BS. Whole-body organ-level and kidney micro-dosimetric evaluations of ^{64}Cu-loaded HER2/ErbB2-targeted liposomal doxorubicin ^{64}Cu-MM-302 in rodents and primates. EJNMMI Res. 2015;5:24. [PubMed: 25918676]
33. Baxter LT, Zhu H, Mackensen DG, Butler WF, Jain RK. Biodistribution of monoclonal antibodies: scale-up from mouse to human using a physiologically based pharmacokinetic model. Cancer Res. 1995;55:4611–22. [PubMed: 7553638]
34. Gabizon AA, Tzemach D, Mak L, Bronstein M, Horowitz AT. Dose dependency of pharmacokinetics and therapeutic efficacy of pegylated liposomal doxorubicin (DOXIL) in murine models. J Drug Target. 2002;10:539–48. [PubMed: 12683721]
35. Jokerst JV, Lobovkina T, Zare RN, Gambhir SS. Nanoparticle PEGylation for imaging and therapy. Nanomedicine (Lond). 2011;6:715–28. [PubMed: 21718180]
36. Delille J-P, Slanetz PJ, Yeh ED, Kopans DB, Garrido L. Breast cancer: regional blood flow and blood volume measured with magnetic susceptibility-based MR imaging--initial results. Radiology. 2002;223:558–65. [PubMed: 11997568]
37. Jain RK. Determinants of tumor blood flow: a review. Cancer Res. 1988;48:2641–58. [PubMed: 3282647]
38. Brix G, Bahner ML, Hoffmann U, Horvath A, Schreiber W. Regional blood flow, capillary permeability, and compartmental volumes: measurement with dynamic CT--initial experience. Radiology. 1999;210:269–76. [PubMed: 9885619]
39. Maeda H. Macromolecular therapeutics in cancer treatment: the EPR effect and beyond. J Control Release. 2012;164:138–44. [PubMed: 22595146]
40. Koukourakis MI, Koukouraki S, Giatromanolaki A, Kakolyris S, Georgoulias V, Velidaki A, et al. High intratumoral accumulation of stealth liposomal doxorubicin in sarcomas--rationale for combination with radiotherapy. Acta Oncol. 2000;39:207–11. [PubMed: 10859012]

41. Koukourakis MI, Koukouraki S, Fezoulidis I, Kelekis N, Kyrias G, Archimandritis S, et al. High intratumoural accumulation of stealth liposomal doxorubicin (Caelyx) in glioblastomas and in metastatic brain tumours. Br J Cancer. 2000;83:1281–6. [PubMed: 11044350]

42. Arrieta O, Medina L a, Estrada-Lobato E, Hernández-Pedro N, Villanueva-Rodríguez G, Martínez-Barrera L, et al. First-line chemotherapy with liposomal doxorubicin plus cisplatin for patients with advanced malignant pleural mesothelioma: phase II trial. Br J Cancer. 2012;106:1027–32. [PubMed: 22353806]

43. Arrieta O, Medina L-A, Estrada-Lobato E, Ramírez-Tirado L-A, Mendoza-García V-O, de la Garza-Salazar J. High liposomal doxorubicin tumour tissue distribution, as determined by radiopharmaceutical labelling with (99m)Tc-LD, is associated with the response and survival of patients with unresectable pleural mesothelioma treated with a combination of liposomal. Cancer Chemother Pharmacol. 2014;74:211–5. [PubMed: 24817602]

44. Bae YH, Park K. Targeted drug delivery to tumors: myths, reality and possibility. J Control Release. 2011;153:198–205. [PubMed: 21663778]

45. Nichols JW, Bae YH. Odyssey of a cancer nanoparticle: from injection site to site of action. Nano Today. 2012;7:606–18. [PubMed: 23243460]

46. Tamura K, Kurihara H, Yonemori K, Tsuda H, Suzuki J, Kono Y, et al. ^{64}Cu-DOTA-Trastuzumab PET Imaging in Patients with HER2-Positive Breast Cancer. J Nucl Med. 2013;1–7.

47. Dijkers EC, Oude Munnink TH, Kosterink JG, Brouwers a H, Jager PL, de Jong JR, et al. Biodistribution of 89Zr-trastuzumab and PET imaging of HER2-positive lesions in patients with metastatic breast cancer. Clin Pharmacol Ther. 2010;87:586–92. [PubMed: 20357763]

48. Siegal T, Horowitz a, Gabizon AA. Doxorubicin encapsulated in sterically stabilized liposomes for the treatment of a brain tumor model: biodistribution and therapeutic efficacy. J Neurosurg. 1995;83:1029–37. [PubMed: 7490617]

49. Lockman PR, Mittapalli RK, Taskar KS, Rudraraju V, Gril B, Bohn KA, et al. Heterogeneous blood-tumor barrier permeability determines drug efficacy in experimental brain metastases of breast cancer. Clin Cancer Res. 2010;16:5664–78. [PubMed: 20829328]

50. Sharma US, Sharma A, Chau RI, Straubinger RM. Liposome-mediated therapy of intracranial brain tumors in a rat model. Pharm Res. 1997;14:992–8. [PubMed: 9279878]

Statement of Translational Relevance:

The field of nanomedicine has highly debated the presence and extent of the enhanced permeability and retention (EPR) effect in human tumors, a key mechanistic hallmark for nanomedicine to achieve effective drug delivery and subsequent therapeutic benefits. In this translational study, ^{64}Cu-labeled HER2-targeted liposomal doxorubicin was quantified by positron emission tomography (PET) and found to accumulate in human tumors. Based on ^{64}Cu-PET quantification, the range of tumor drug concentrations is predicted to result in variable anti-tumor activity. High tumor deposition was stratified based on a cutoff that is consistent with preclinical studies, and was associated with more favorable treatment outcome. This suggests that a nanoparticle imaging approach may be applicable as a biomarker strategy for personalizing nanomedicines.

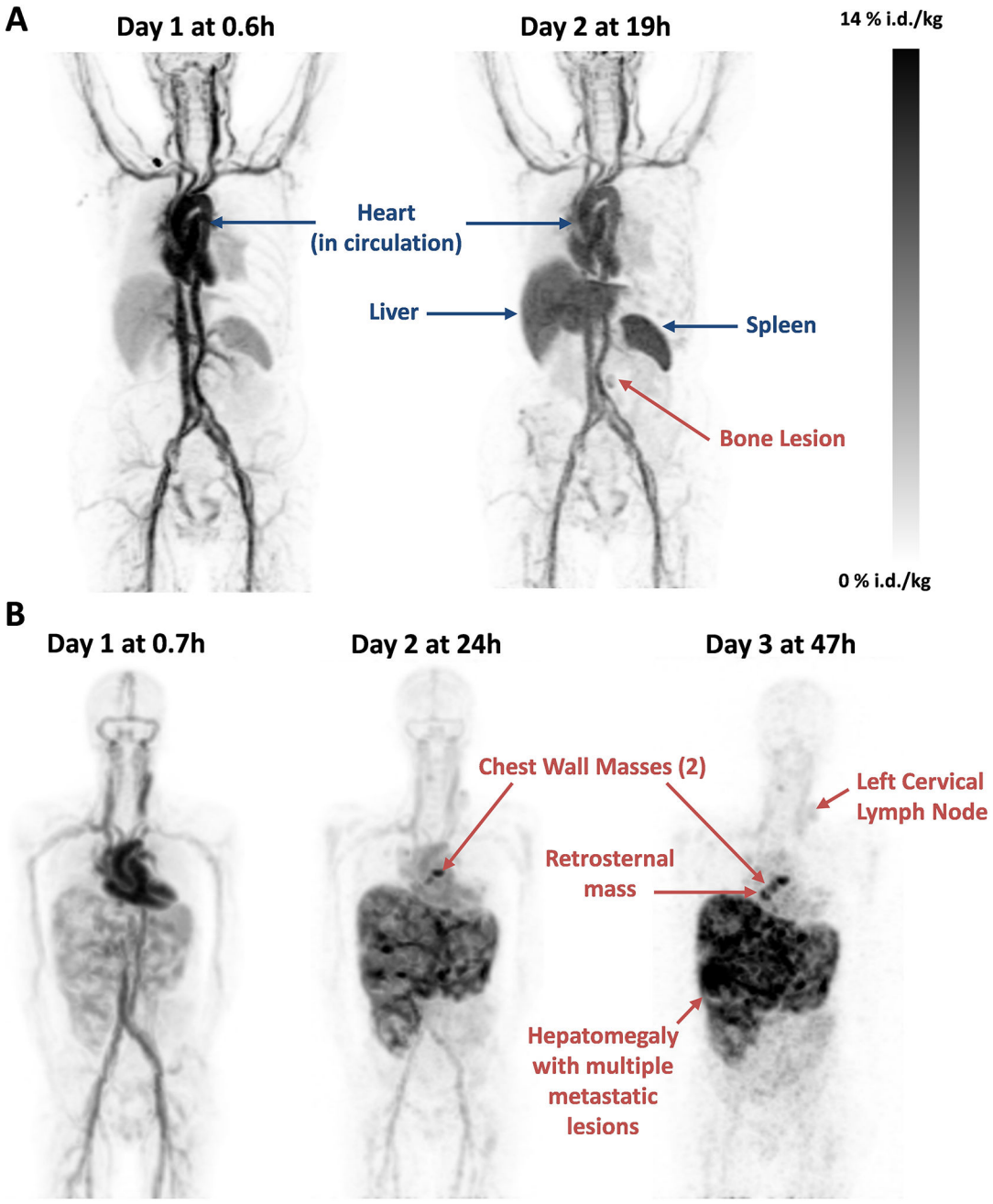

Fig. 1. Biodistribution of ^{64}Cu-MM-302 in patients.

Maximum-intensity-projection PET images of two patients with HER2-positive breast cancer injected with 30 mg/m^2 of MM-302 and a tracer dose of ^{64}Cu-MM-302 (400 MBq). PET/CT Images were acquired at **(A)** 0.6 and 19 h post-injection in Patient 02, and **(B)** 0.7, 24, and 47 h post-injection in Patient 06. Immediately post-administration, ^{64}Cu-MM-302 activity was primarily confined in the blood pool because of the extended circulation property of liposomes. On Days 2 and 3, ^{64}Cu-MM-302 uptake was evident in normal spleen and liver, as well as in various tumor lesions.

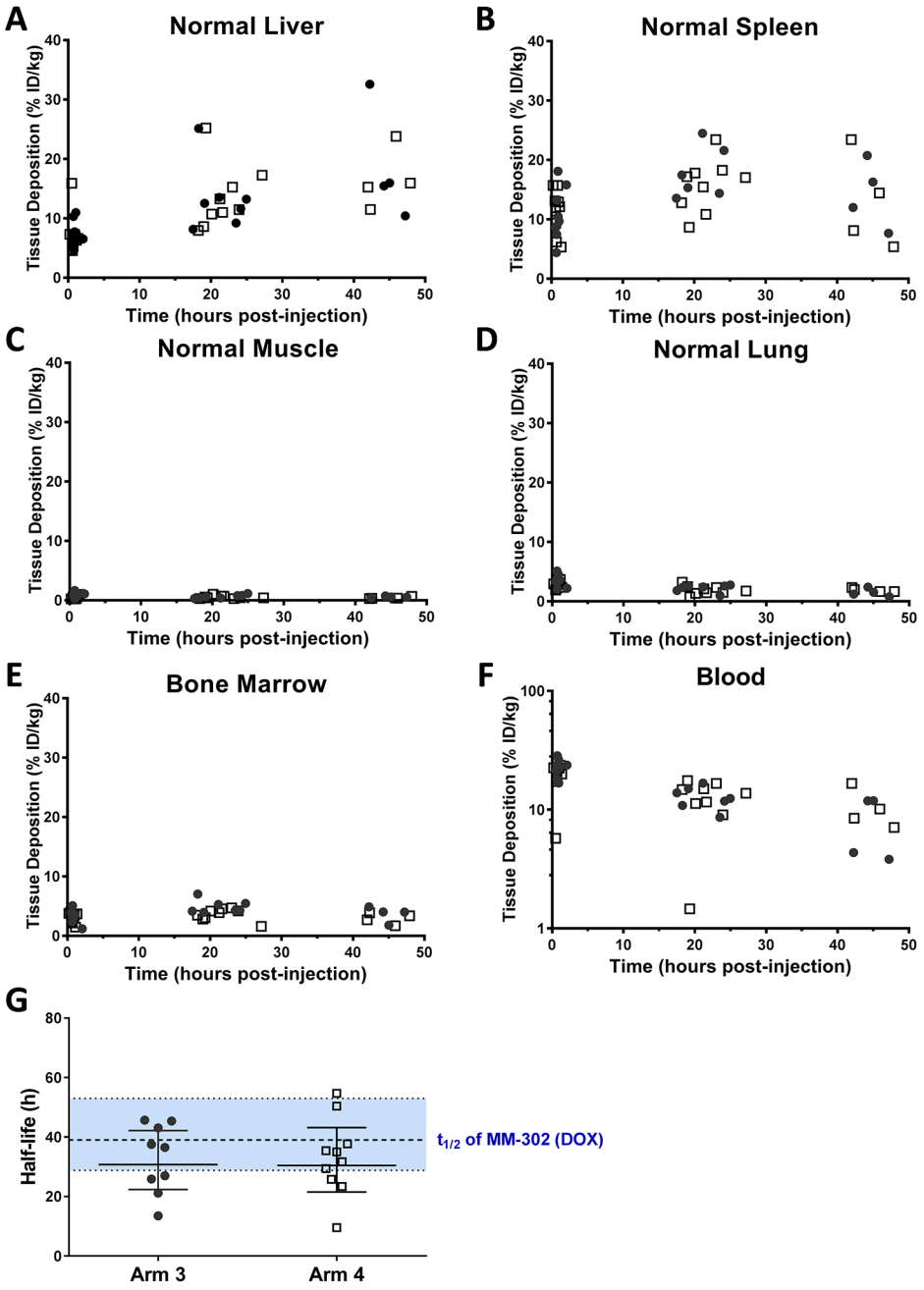

Fig. 2. Tissue deposition kinetics of ^{64}Cu-MM-302.

Image-based quantification of ^{64}Cu-MM-302 normal tissue deposition kinetics in HER2-positive breast cancer patients. A spherical ROI was drawn in normal tissues on the PET/CT images to obtain SUV_{median} for **(A)** liver, **(B)** spleen, **(C)** muscle (quadriceps), **(D)** lung, **(E)** bone marrow, and **(F)** aorta (blood). Deposition of ^{64}Cu-MM-302 is expressed as percentage of injected dose per kilogram of tissue (%ID/kg) and is decay corrected. **(G)** Circulation half-life of ^{64}Cu-MM-302 for individual patients was fit with a one-compartment model. The shaded area represents $t_{1/2}$ (geometric mean, with 95% CI) obtained from Phase 1 MM-302 PK study by measuring doxorubicin content in the patient plasma at 30 mg/m^2.

Closed and open symbols represent patient data in Arm 3 (no cyclophosphamide) and Arm 4 (with cyclophosphamide) of the Phase 1 study, respectively.

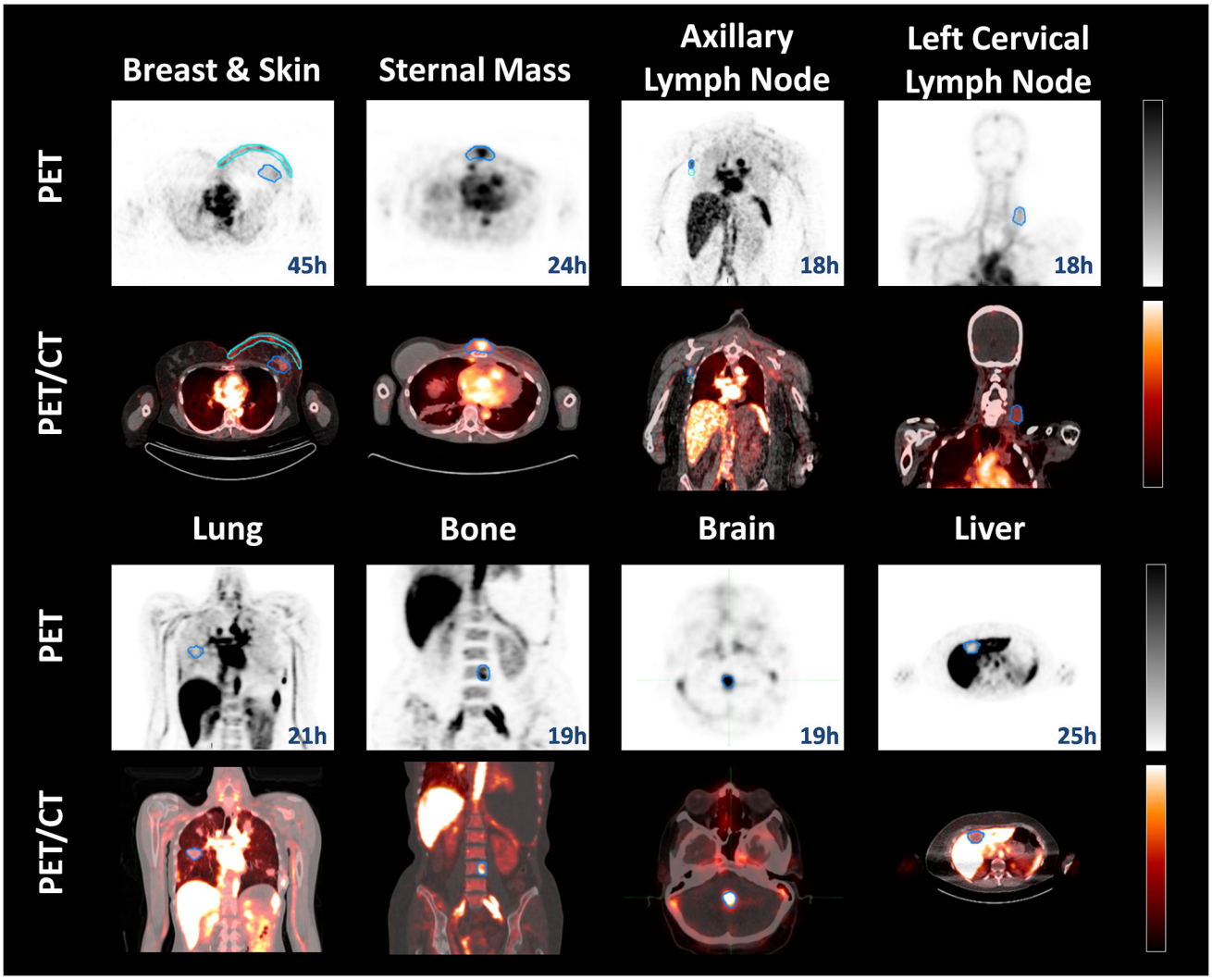

Fig. 3. Visualization of ^{64}Cu-MM-302 lesion deposition.

Representative PET and fused PET/CT images of ^{64}Cu-MM-302 in lesions at different anatomical locations. Intensity scale bars represent deposition from 0 to 10 %ID/kg (derived from SUV_{median}). The regions of interest used to measure tumor deposition of ^{64}Cu-MM-302 are shown in blue or turquoise outlines. ^{64}Cu-MM-302 uptake was detected at above muscle background level in lesions of various anatomical locations that are common for HER2-positive metastatic diseases.

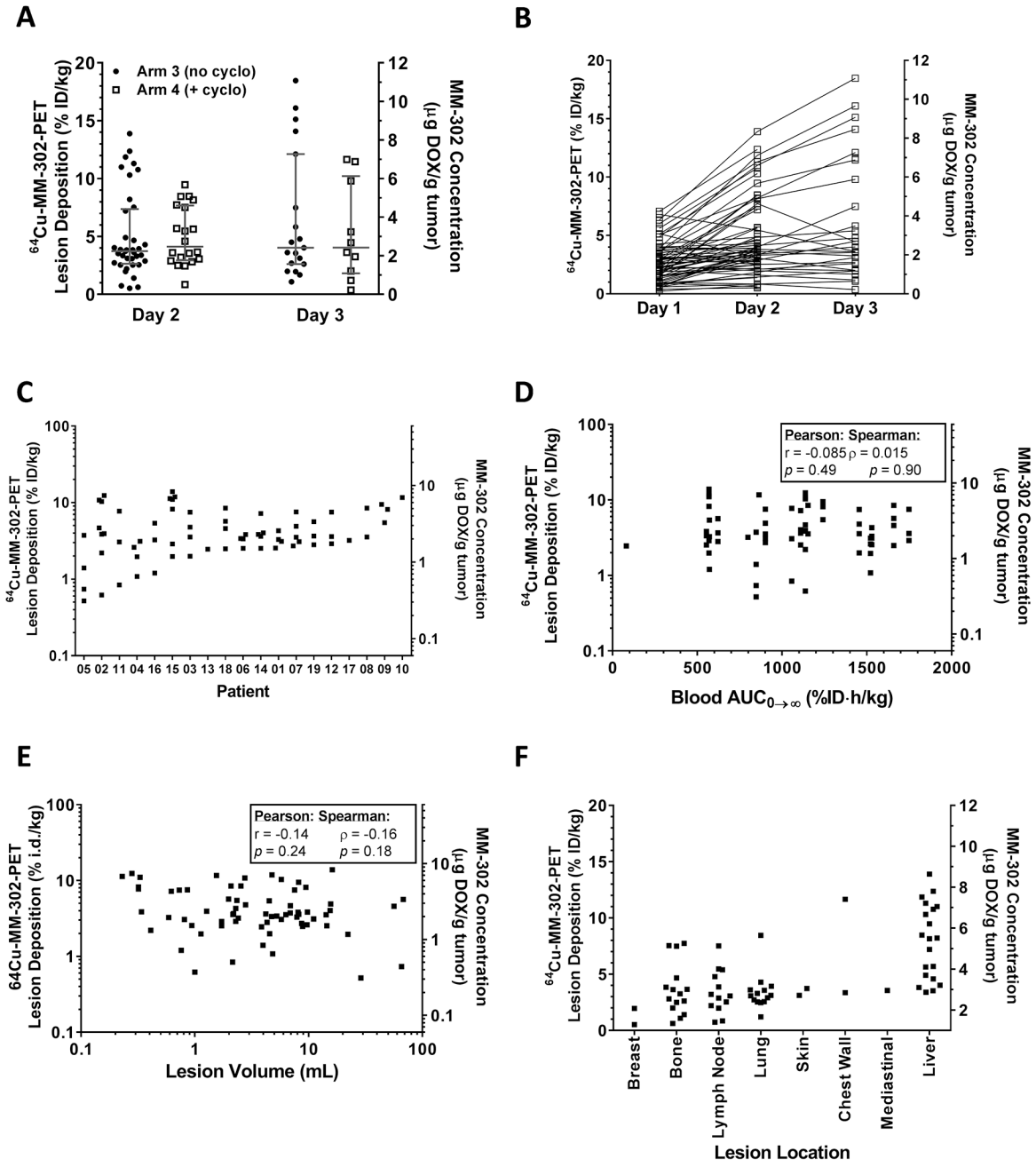

Fig. 4. Quantification of ^{64}Cu-MM-302 uptake in tumor lesions.

(A) Lesion uptake of ^{64}Cu-MM-302 in patients on Days 2 and 3 in patients treated with (open square) and without (closed circle) cyclophosphamide (cyclo). No significant difference in lesion deposition was observed between the two treatment groups ($p \geq 0.67$, Mann-Whitney test). **(B)** ^{64}Cu-MM-302 deposition kinetics in all patient lesions illustrating accumulation of MM-302 in lesions from Day 1 to 3. Statistical difference in lesion uptake was only detectable from Day 1 ($p < 0.0001$, ANOVA), but not between Days 2 and 3 ($p > 0.67$). **(C)** Tumor deposition of ^{64}Cu-MM-302 in individual patients was shown to be highly variable. No correlation of tumor deposition was detected with **(D)** blood exposure or **(E)**

tumor size. **(F)** ^{64}Cu-MM-302 deposition in lesions of different anatomical locations. Panels (C–F) include data obtained on Day 2, or Day 3 if patient did not undergo PET scan on Day 2.

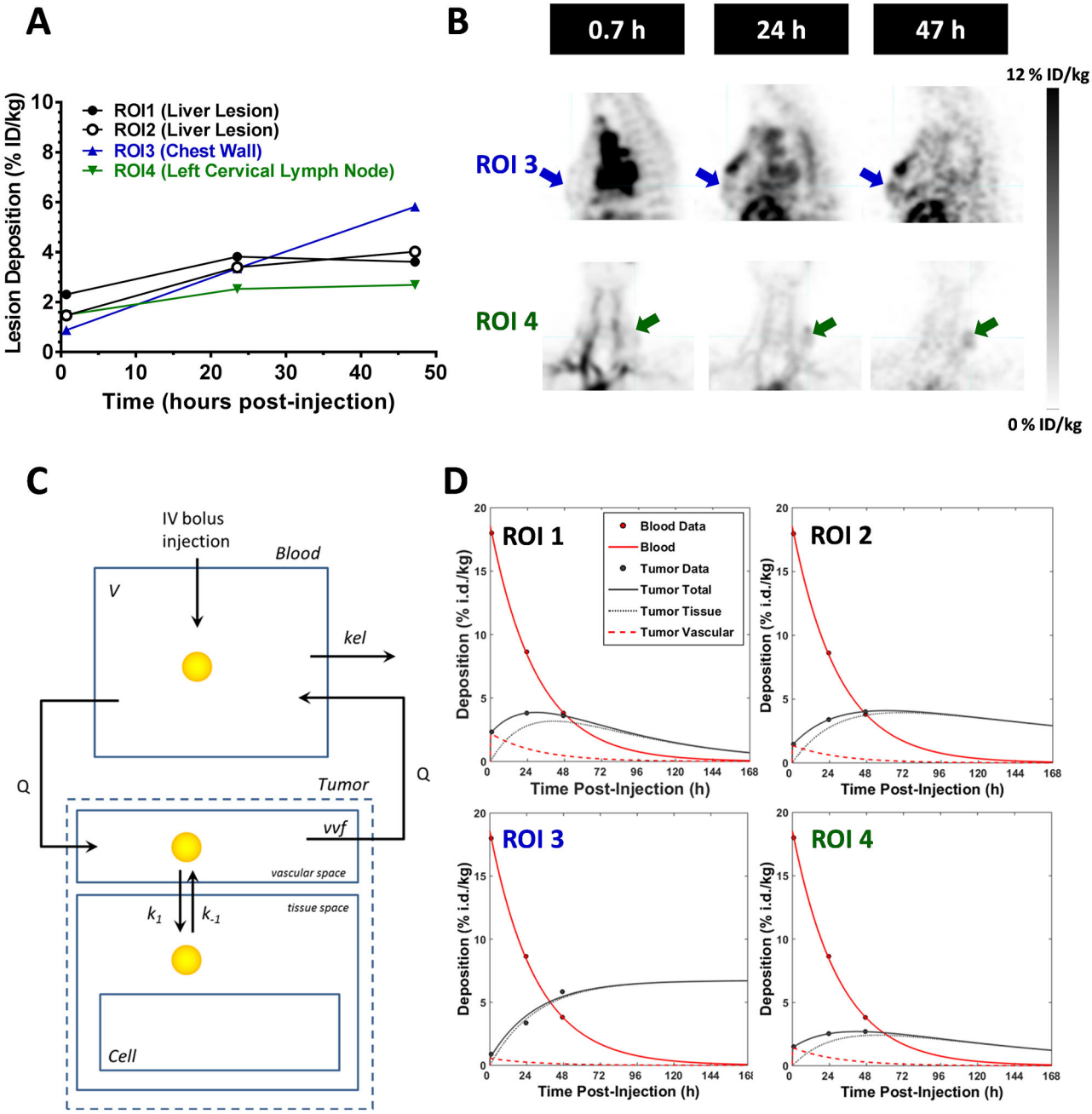

Fig. 5. Kinetics of ^{64}Cu-MM-302 deposition in tumor lesions.

Lesion deposition kinetics of ^{64}Cu-MM-302 in a HER2-positive breast cancer patient who received 3 PET/CT scans at 0.7 h, 24 h, and 47 h post-injection (Patient 06). **(A)** Lesion deposition for each ROI is expressed as %ID/kg derived from SUV_{median} (decay-corrected). **(B)** Sagittal view of PET images illustrating deposition in ROI 3 (chest wall mass) and ROI 4 (left cervical lymph node). **(C)** Schematic diagram of PK model describing ^{64}Cu-MM-302 transport kinetics post-injection. **(D)** Blood and lesion deposition data fit to the model described in (C), illustrating ^{64}Cu signal contribution kinetics from tumor vascular vs. tumor tissue compartments at 0 to 168 h post-injection.

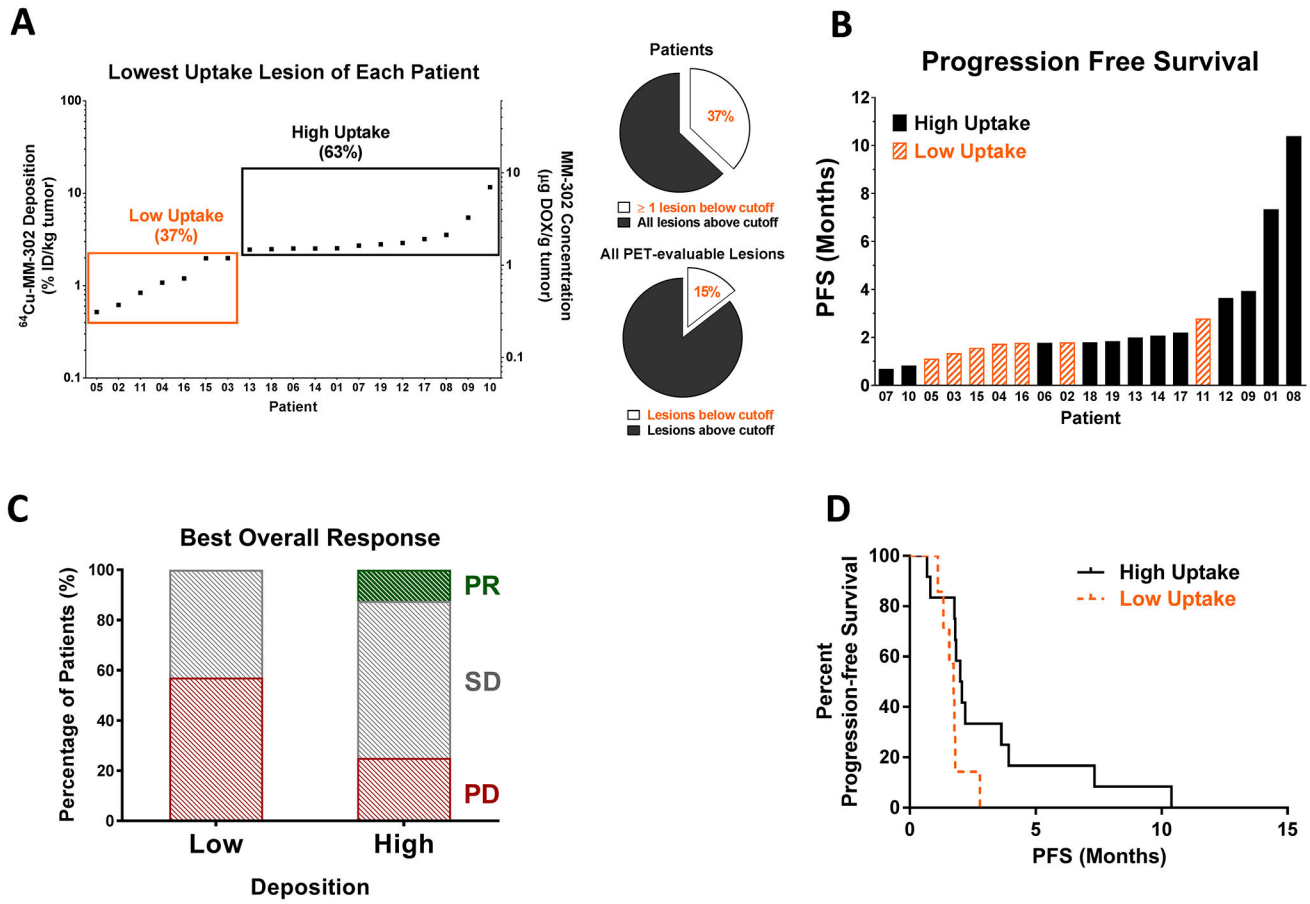

Fig. 6. Patient treatment outcome stratified by deposition of lowest uptake lesion.

(A) ^{64}Cu-MM-302 lesion deposition of the lowest uptake lesion within each patient from Days 2 or 3 are shown and aligned in ascending order. A deposition threshold was selected based on the inflection point of the deposition graph and confirmed by ROC analysis, where patients to the left of the inflection point were designated as “low uptake” group. The inset figures illustrate the percentage of patients with >1 lesion that are below or above the cutoff (top inset), and percentage of lesions that are below or above the cutoff (bottom inset). PFS of the imaged patients are shown in **(B)**, where “low uptake” patients are depicted with orange striped bars, and “high uptake” patients are depicted with black solid bars. The best overall response per RECIST v1.1 criteria was captured in **(C)** stratified into the “low uptake” and “high uptake” groups, where PR, SD, and PD represent partial response, stable disease, and progressive disease, respectively. **(D)** Patient PFS of the high vs. low uptake patients were shown in a Kaplan-Meier curve.